Failure analysis of leakage on titanium tubes within heat exchangers in a nuclear power plant. Part I: Electrochemical corrosion

Z.-G. Yang*, Y. Gong and J.-Z. Yuan

Titanium tubes generally exhibit superior resistance against electrochemical corrosions amid seawater for their passive films TiO_2. However, hydrogen-assisted corrosion (HAC) is actually the Achilles' heel to titanium materials when the temperature exceeds near 70 °C. In this event, severe degradations like quick thinning and leakage were frequently detected on a large number of titanium tubes exposed to natural seawater environment within heat exchangers in a nuclear power plant, which caused serious safety problems. This paper is the Part I of totally two parts conducted for the whole failure analysis study, mainly focusing on electrochemical aspect of failure causes and their behaviors. By means of over ten kinds of characterization methods, the analysis results identified that the HAC induced by the interaction effects between galvanic corrosion and crevice corrosion led to local bulges of the inner walls of some titanium tubes, and then the bulges were quickly thinned and eventually ruptured under the eddy erosion from the seawater containing sediment particles. Finally, relevant mechanisms were addressed in detail and prevention methods were proposed as well.

1 Introduction

Among all the thirteen nuclear power units presently under operation in China [1, 2], the two 728MWe CANDU 6 units in the Phase III of Qinshan Nuclear Power Plant, which were imported from Atomic Energy of Canada Limited (AECL), are the first and the only two pressurized heavy water reactor (PHWR) units in China, and started commercial operation on 31 December 2002 and 24 July 2003, respectively, with design lifetime of 40 years [3].

In a CANDU 6 style unit, the recirculating cooling water (RCW) system consists of two heat exchange loops – the first one cools the power equipments in the nuclear island and the steam equipments in the conventional island by means of desalinated water, while the second one cools such warmed desalinated water by using natural seawater within a specific kind of equipment called RCW heat exchanger [4]. Hereby, each of the two CANDU 6 units is equipped in the conventional island with four shell and tube [5] RCW heat exchangers, within which the desalinated water is conveyed outside the tubes (also called the shell side), and the seawater is transported inside the tubes (also called the tube side). However, natural seawater usually contains high contents of salts, chloride ions, and even sediment particles, various selective corrosions as well as mechanical degradations are consequently prone to emerge on these heat exchanger tubes with matrix of titanium, greatly reducing their service lifetimes.

In this event, during about 3 years after actual operation (2003–2006), failure incidents including clogging, quick thinning, and even leakage, etc. frequently occurred on a great number of titanium tubes within the RCW heat exchangers of the two CANDU 6 nuclear power units in Qinshan Phase III, causing substantial economic losses as well as potential safety problems [6]. Materials quality, equipment operation, service environment, routine maintenance, or other factors, which were the main causes for inducing these premature failures in these cooling equipment, were urgently investigated. Consequently, in order to immediately identify the causes of such failures, investigations into four aspects were carried out by referencing our previous successful failure analysis experiences [7–9], including matrix materials, environmental media, operation conditions, installation, and maintenance. Based on the leaked tubes and the environmental media as seawater, desalinated water, etc., over 10 kinds of characterization methods were conducted for failure analysis in series of totally two parts, and totally seven kinds of

Z.-G. Yang, Y. Gong
Department of Materials Science, Fudan University, Shanghai 200433 (P.R. China)
E-mail: zgyang@fudan.edu.cn

J.-Z. Yuan
Third Qinshan Nuclear Power Co. Ltd., Haiyan 314300, Zhejiang Province (P.R. China)

different failure mechanisms were simultaneously detected. As a matter of fact, such a comprehensive failure analysis study from engineering practice for titanium tubes that are applied in nuclear power units has been rarely reported. In the Part I of this whole study, research mainly focused on the electrochemical corrosion on the titanium tubes, while in the Part II [10], analysis dominantly concentrated in the mechanical degradation on the tubes. Concretely in this paper addressed for the Part I, the hydrogen-assisted corrosion (HAC) including both hydrogen blistering (HB) and hydrogen embrittlement (HE), which is generally thought to emerge on titanium only above temperature of 70 °C [11], was actually found occurring around 35–40 °C when it was induced by the interaction effect between galvanic corrosion and crevice corrosion under complicated service conditions. Relevant mechanisms of these electrochemical corrosions, especially their interaction effect were discussed in detail. Finally, countermeasures and suggestions were also put forward.

2 Experimental

2.1 Visual observation

As shown in Fig. 1(a), the RCW heat exchanger is a horizontal cylinder with dimension of about $\varphi 2400 \times 15\,000$ mm, in which there exist totally 4932 tubes (ASME SB-338 Gr.2 titanium [12], $\varphi 19 \times 14\,630 \times 0.71$ mm) in 57 rows and 93 columns. All the tubes are sustained by 23 16 mm-thick carbon steel baffle plates with interval distance of 603 mm, and their two ends were hydraulically expanded (expansion ratio 80%) with carbon steel tube sheets cladded by titanium (ASME SA-515 Gr.65 carbon steel [13] 78 mm-thick, ASME SB-265 Gr.1 Ti [14] 3 mm-thick), without seal welding. Therein, the diameter of supporting holes on all the plates was 19.25 ± 0.51 mm. The schematic diagram of the RCW heat exchanger, as well as the working parameters including flow directions and input/output temperatures of the desalinated water and seawater are all listed in Fig. 1(b).

The two target leaked tubes analyzed in the present study were both sampled from the 4# RCW heat exchanger of unit II, which suffered the severest degradations on its tubes among all the eight heat exchangers in the two CANDU 6 units – 113 tubes were found to be heavily thinned, and another 24 tubes were even leaked. Furthermore, the ruptures on over 90% of the leaked tubes were located between the first baffle plate and the 78 mm-thick tube sheet, and even buried inside this tube sheet, also seen in Fig. 1(b). Meanwhile, as indicated with the circles in Fig. 2, obvious brown corrosion phenomenon was observed on the surface of the tube sheet itself as well.

Figure 3 presents the external appearances of the two leaked tubes named A and B from this heat exchanger. As shown in Fig. 3(a), the rupture on tube A was in shape of 5×3 mm ellipse and located about 30 mm off the inlet. While for the rupture on tube B, it seemed relatively round with a diameter of nearly 6 mm, and was 70 mm off the inlet, seen in Fig. 3(b). Hereby, it must be noted that both the distances of the two ruptures off the tube inlets were less than 78 mm, i.e., they were both formed buried inside the tube sheet.

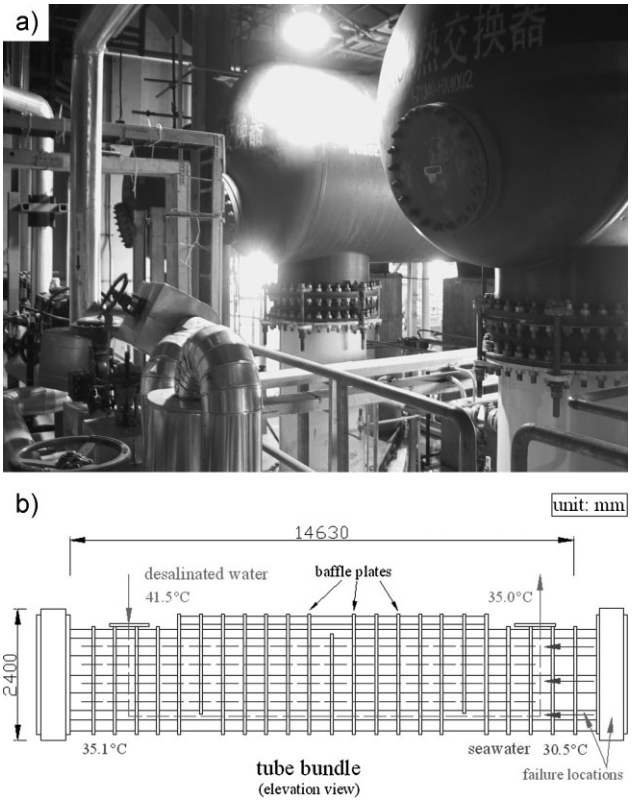

Figure 1. Illustration of the RCW heat exchanger: (a) external appearance, (b) scheme and operation parameters

2.2 Characterization methods

Then investigations from three aspects were successively carried out on the two leaked tubes, including the evaluation of their matrix materials, the inspection of the two media they contacted (i.e., desalinated water and seawater), and the microscopic analysis of the ruptures on them. As for the first one, oxygen nitrogen hydrogen (ONH) analyzer, carbon sulfur analyzer (CSA), and inductively coupled plasma atomic emission spectroscopy (ICP-AES), were used to inspect their chemical compositions; optical microscopy (OM) was utilized to observe their metallographic structures; and series of mechanical tests including

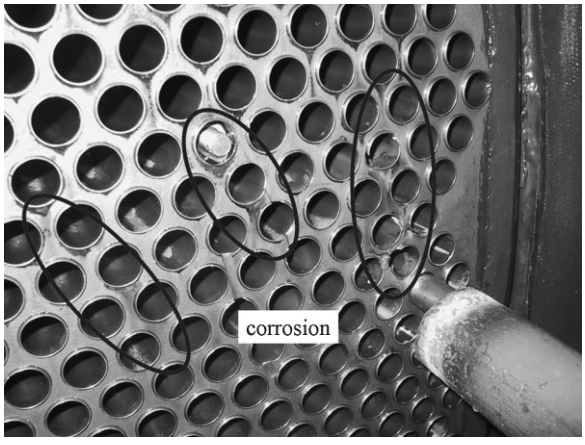

Figure 2. Corrosion on the inlet of the tube sheet

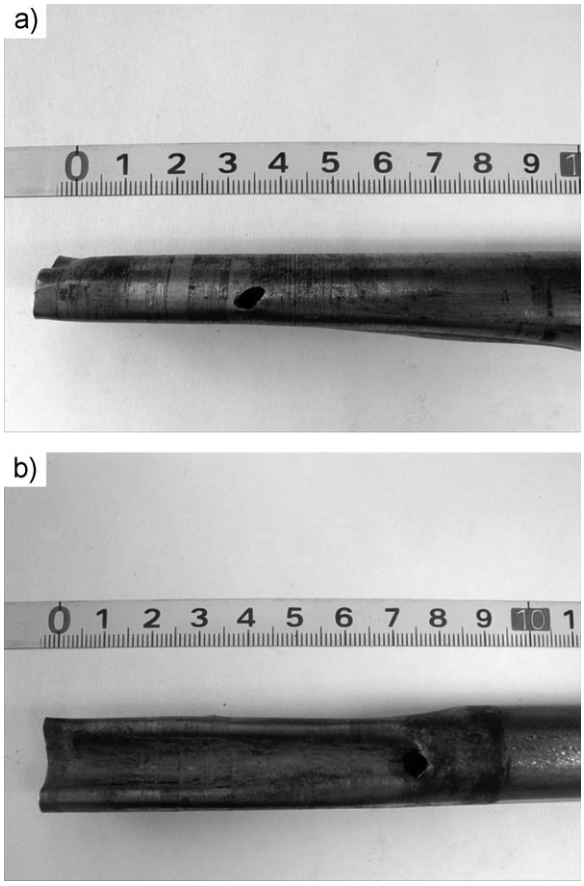

Figure 3. External appearances of the ruptures on the two leaked tubes: (a) tube A, (b) tube B

tensile test, hardness survey, etc. were also applied to evaluate their mechanical properties. With respect to the second one, the chemical constituents of the desalinated water and the seawater were respectively detected by graphite furnace atomic absorption spectrometry (GFAAS), ion chromatography (IC), and ICP-AES. In terms of the final one, besides further observation of the macroscopic morphologies of the ruptures on the two leaked tubes in Fig. 3, scanning electron microscopy (SEM) and energy dispersive spectrometry (EDS) were adopted to analyze their microscopic morphologies along with micro-area compositions; meanwhile, X-ray photoelectron spectroscopy (XPS), secondary ion mass spectrometry (SIMS), and X-ray diffraction (XRD) were also employed to characterize their near-surface features.

3 Results and discussion

3.1 Matrix materials

3.1.1 Chemical compositions

Chemical compositions of the titanium tubes' matrix materials are listed in Table 1, which are in accordance with the requirements of the ASME SB-338 Gr.2 titanium specification (equals to the TA2 industrial purity titanium in GB/T 3620.1-2007 standard of China [15]), as well as their original values provided by manufacturer RMI. In fact, contents of some of the impurities are even nearly one order of magnitude less than their limitations.

3.1.2 Metallographic structures

Figure 4(a) and (b) show the metallographic structures of the titanium tubes in, respectively, transverse and longitudinal directions. It is obvious that the structures in both directions display a similar morphology, i.e., equiaxed polygonal grains – the typical structure of α-titanium, and their average ASTM grain size is about 8. It should be also pointed out that the sizes of these grains are basically even, without excessively coarsened or fined.

3.1.3 Mechanical test

In order to examine whether performances deterioration had occurred on the titanium tubes, various mechanical tests were conducted on the two leaked tubes, and the results were also compared with the original values after manufacture. As listed in Table 2, all the mechanical properties of the tubes were still eligible according to their standards, and the yield strength and the tensile strength were even a bit increased than the original values.

Based on all the analysis results illustrated above, it can be concluded now that the matrix materials of the titanium tubes after service were still qualified, in other words, the failures could not be ascribed to the inappropriate selection of tube materials.

3.2 Environmental media

In this section, inspection will be mainly focused on the two kinds of liquids, the desalinated water and the seawater. Since the concentrations of the constituents in the desalinated water were quite low, GFAAS was particularly adopted, and the results were listed in Table 3. It should be noted that the contents of iron and copper elements were relatively high, which means that corrosion had exactly occurred in the RCW system. With respect to the seawater, by using ICP-AES and IC, its element constituents were

Table 1. Chemical compositions of the titanium tubes (wt%)

Element	Fe	C	N	H	O	Others	
						Single	Total
tube in 4# of Unit II	0.069	0.012	0.006	0.0019	0.12	/	/
original values from RMI	0.07	0.01	0.008	0.0015	0.12	/	/
ASME SB-338 Gr.2	≤0.30	≤0.08	≤0.03	≤0.015	≤0.25	≤0.10	≤0.40
GB/T 3620.1-2007 TA2	≤0.30	≤0.08	≤0.03	≤0.015	≤0.25	≤0.10	≤0.40

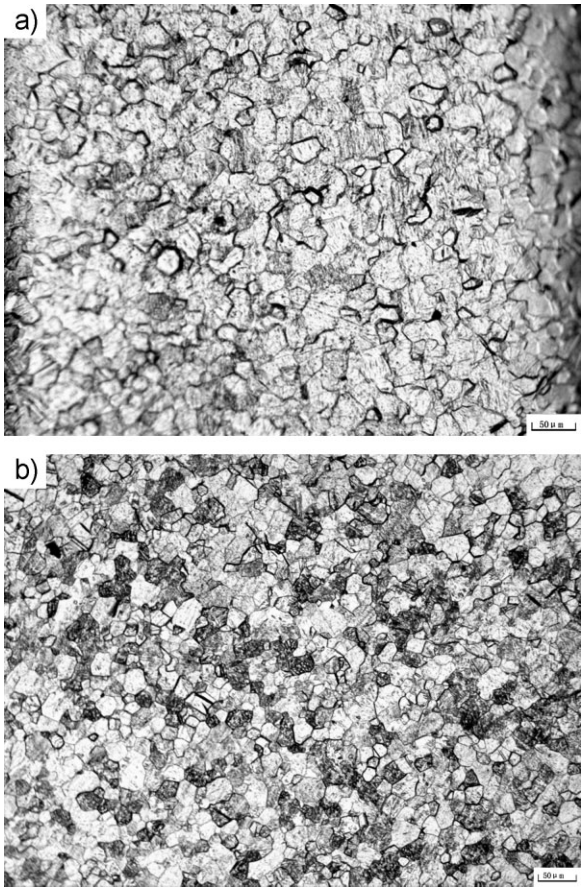

Figure 4. Metallographic structures of the titanium tubes: (a) transverse, (b) longitudinal

revealed in Table 4, which conformed to the normal compositions of natural seawater – a high content of chloride ions.

3.3 Rupture analysis of tube A

3.3.1 SEM and EDS

After magnifying the rupture in Fig. 3(a), it can be obviously learnt from Fig. 5(a) that the fringes of this rupture were bent inwards to the inside wall, which may be attributed to a relatively large force exerting on the outside wall of the tube. Meanwhile, brown colored rust covered around this rupture, which should be the corrosion products of iron oxides originated from the Ti/carbon steel tube sheet. The inside wall around the rupture was pretty smooth, and the extent of rusting was not as severe as that on the outside wall too [Fig. 5(b)].

Under SEM, microscopic morphology of the area marked with rectangular in Fig. 5(b) was presented in Fig. 6(a). Besides the smooth fringe (site 001), some corrosion substances (site 002) were also scaling on the inside wall of the rupture. By means of EDS, the former one was exactly the titanium matrix material of the tube [Fig. 6(c)], while the latter one actually also contained iron and oxygen elements other than titanium [Fig. 6(d)]. It can be inferred that such corrosion substances were introduced from the outside wall of the tube after the rupture was formed. Furthermore, it must be particularly noted that the corner of the inside wall exhibited an unusual morphology seeming like oriented eddy erosion, seen in Fig. 6(b). Just due to this erosion effect, almost no corrosion substances were scaling around the corner, completely contrast to the site 002 in Fig. 6(a). Also, another significant evidence also revealed that densely distributed pits existed near the corner with eddy erosion trace. This fact means that such kind of erosion was even accompanied with impact because of the sediment particles contained in the natural

Table 2. Mechanical properties of the titanium tubes (wt%)

	Yield strength $\sigma_{0.2}$ (MPa)	Tensile strength σ_b (MPa)	Elongation δ_5 (%)	Hardness HV1
Sample 1	435	535	35.0	174
Sample 2	427	545	31.5	166
Average	431	540	33.3	170
original values from RMI	296–351	435–494	32–39	/
ASME SB-338 Gr.2	275–450	$\geq$ 345	$\geq$ 20	/
GB/T 3624-1995[16]	$\geq$250	370–530	$\geq$20	165–225

Table 3. GFAAS results of the desalinated water (ppb, equals to μg/L)

Element	Fe	Cu	Ti	Mn	Ni	Cr
desalinated water	137	39.2	<20	2.5	<5	0.7

Table 4. Element constituents of the seawater (ppm, equals to mg/L)

Element	Cl	Mg	Al	Cu	Fe	Ti	Mn
Seawater	5.19×10^3	1.16×10^2	0.13	<0.002	0.088	<0.002	0.015

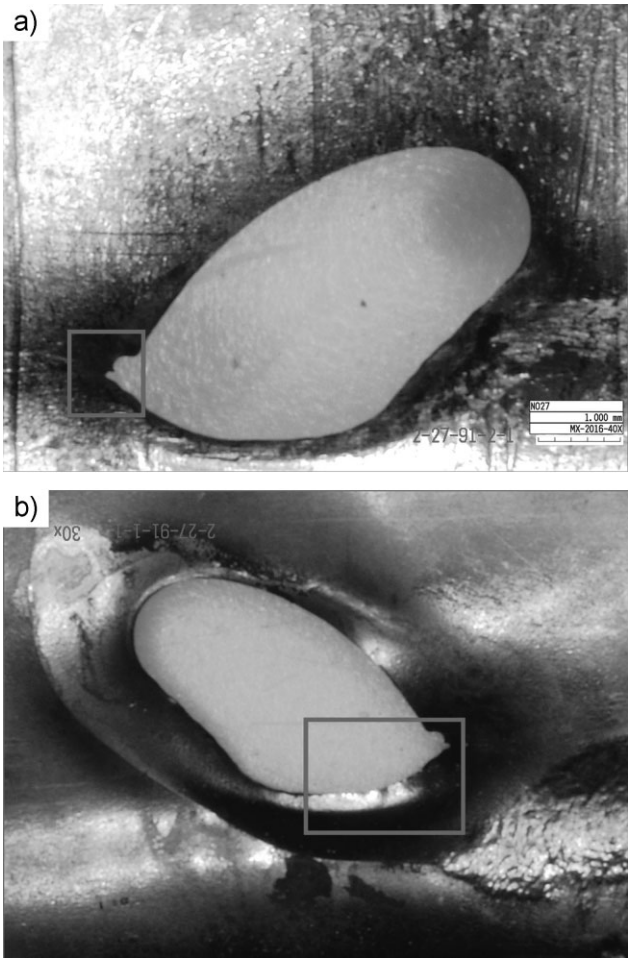

Figure 5. Macroscopic morphologies of the rupture on tube A: (a) outside wall, (b) inside wall

seawater, whose mechanism will be detailedly discussed in Part II of this study.

3.3.2 XPS

For the purpose of characterizing the surface features of both the outside wall and the inside wall near the rupture, XPS was utilized to determine the chemical valences of relevant elements. As shown in Fig. 7(a), totally four kinds of main elements were present on the outside wall, among them the two metal elements should be paid special attention to since they were from the matrix materials of the tube and the plate. The electron binding energy of iron was 711.80 eV, which corresponded to the compound FeO(OH) [17]. However for titanium, it had two close spectra, that is to say two species of chemical valences existed. After locally magnifying [Fig. 7(b)], the binding energy of the left one was 458.48 eV, while that of the right one was 455.74 eV. Referring to the handbook [17], the former one represented TiO_2, however the latter one could not correspond to any compound. In other words, an irregular chemical valence was introduced on the titanium due to corrosion, and needed subsequent analysis.

In order for comparison, the inside wall near the rupture was also detected by XPS. The binding energy of iron was still 711.80 eV, i.e., the FeO(OH) (Fig. 8); as for the titanium, there was only one titanium spectrum here, and its binding energy was 458.53 eV, i.e., the TiO_2. Now it can be confirmed that some kind of corrosion which would bring about an irregular chemical valence on titanium only occurred on the outside wall of the tube, and was probably related to the unknown force exerting on the tube.

3.3.3 SIMS

Considering the well-known fact that titanium exhibits strong interaction with hydrogen [18], thus the titanium with irregular chemical covalence on the outside wall near the rupture was possibly related to the hydrogen element, which can only be sensitively detected by surface analysis technique SIMS [19]. As displayed in Fig. 9(a), hydrogen element in form of H_2 gas was indeed present, while it did not exist on the inside wall in contrast, seen in Fig. 9(b). This result verified the conclusion we put forward above that corrosion only took place on the outside wall of the tube, and it was very probably the HAC. However, it still needs further method to determine the actual chemical compositions of the titanium hydrides.

3.3.4 XRD

It is clearly shown in Fig. 10 that a kind of crystalline with irregular stoichiometric number as $TiH_{1.924}$ was present other than pure titanium near the rupture. Then, the actual chemical composition of the titanium hydride can be finally ascertained. In fact, the peak of $TiH_{1.924}$ can be regarded as TiH_2 [20], the product of hydrogen absorption reaction.

3.4 Rupture analysis of tube B

3.4.1 Macroscopic morphologies

As shown in Fig. 11(a), a crack with length of 3 mm was engendered from the rupture along the axial direction of the tube and exhibited brittle fracture morphology, while the inside wall near the crack was even seriously deformed, seen in Fig. 11(b). Similar to that on tube A, the rupture fringes here were also bent inwards to the inside wall but with severer extent. So it can be judged that the two ruptures on both tubes A and B were aroused by the same cause, but the degradation extent on tube B was severer than that on tube A.

Consequently, similar microscopic analysis and near-surface characterization were not needed to conduct again on tube B. Instead, cross-sections of the rupture were observed. Figure 12(a) and (b) illustrated that the surface of the outside wall was deteriorated so severe that both delamination and descaling occurred on it, which were the evidence of crevice corrosion. On the contrary, the inside wall of the tube was really smooth, seen in Fig. 12(a). However, the fringe of the rupture was seriously thinned due to the erosion effect from the seawater containing sediment particles, see Fig. 12(c).

4 Failure analysis

Based on the analysis results presented above, it can be concluded from the electrochemical point of view that serious corrosion had occurred on the titanium tubes of the 4# RCW heat exchanger in Unit II. Furthermore, since almost all the rupture locations on the

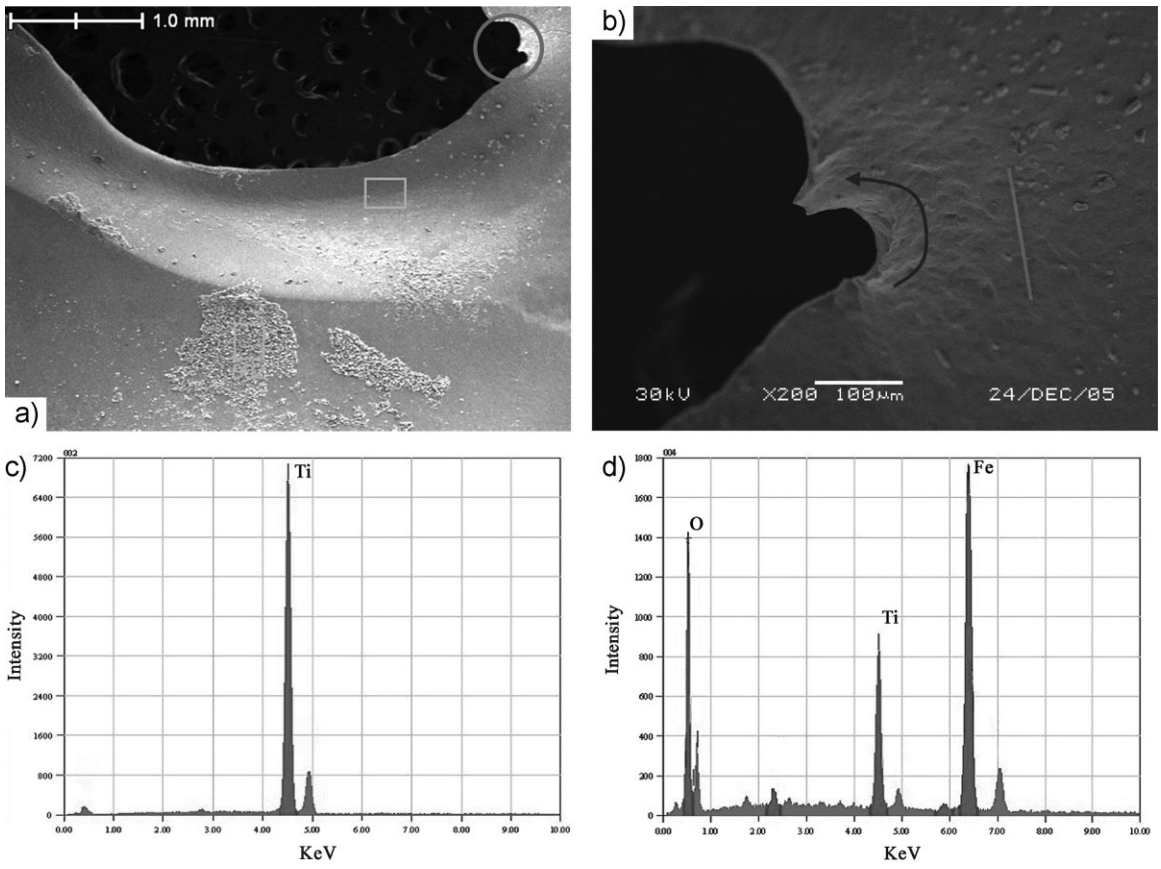

Figure 6. SEM morphologies and EDS of the inside wall of the rupture on tube A: (a) rupture fringe, (b) evidence of eddy erosion, (c) EDS of site 001, (d) EDS of site 002

leaked titanium tubes were buried inside the Ti/carbon steel tube sheet, and also considering the corrosion phenomena in Fig. 2, the galvanic corrosion aroused by the connection of two dissimilar metals as titanium and iron that exhibited different chemical nobilities should be first blamed for.

Generally, the standard electrode potentials of pure titanium and pure iron are −1.63 and −0.44 V, respectively [21], i.e., the titanium will serve as the anode to be corroded when it is in this galvanic pair. However, it is also a common sense that passive film TiO_2 will be spontaneously formed when pure titanium is exposed to the air, and increases the potential. As a result, the potential of titanium shifts to about 0.0 V [22]. In fact, the potential of carbon steel which contains the carbon/iron galvanic pair is also lower than pure iron, at about −0.60 V [22]. Consequently, if the titanium and the carbon steel are connected, carbon steel will act as the anode to be corroded. In this event, such kind of galvanic corrosion was exactly observed on the carbon steel plate in Fig. 2, whose half-cell as well as total reactions are listed in Equation (1), and the schematic diagram is presented in Fig. 13.

$$\begin{aligned} &\text{Anode}: 2Fe \rightarrow 2Fe^{2+} + 4e \\ &\text{Cathode}: O_2 + 2H_2O + 4e \rightarrow 4OH^- \\ &\text{Total reaction}: 2Fe + O_2 + 2H_2O \rightarrow 2Fe(OH)_2 \end{aligned} \quad (1)$$

Then, the corrosion product $Fe(OH)_2$ would continuously react with H_2O and O_2 to be transformed into $Fe(OH)_3$, seen in Equation (2).

$$4Fe(OH)_2 + 2H_2O + O_2 \rightarrow 4Fe(OH)_3 \quad (2)$$

Eventually, various corrosion products like iron oxides and FeO(OH) were formed through Equation (3) to (6), and some of them flaked away from the plate and dropped onto the titanium tube, see the results of XPS, SIMS, and EDS above.

$$Fe(OH)_2 \rightarrow FeO + H_2O \quad (3)$$

$$Fe(OH)_2 + 2Fe(OH)_3 \rightarrow Fe_3O_4 + 4H_2O \quad (4)$$

$$Fe(OH)_3 \rightarrow FeO(OH) + H_2O \quad (5)$$

$$2Fe(OH)_3 \rightarrow Fe_2O_3 + 3H_2O \quad (6)$$

Till now, it may be wondered now that the galvanic corrosion took place on the carbon steel plate, but why the titanium tubes suffered ruptures? Actually, according to the configuration of the RCW heat exchanger, since no seal welding was conducted between the titanium tubes and the sustaining plates, there were

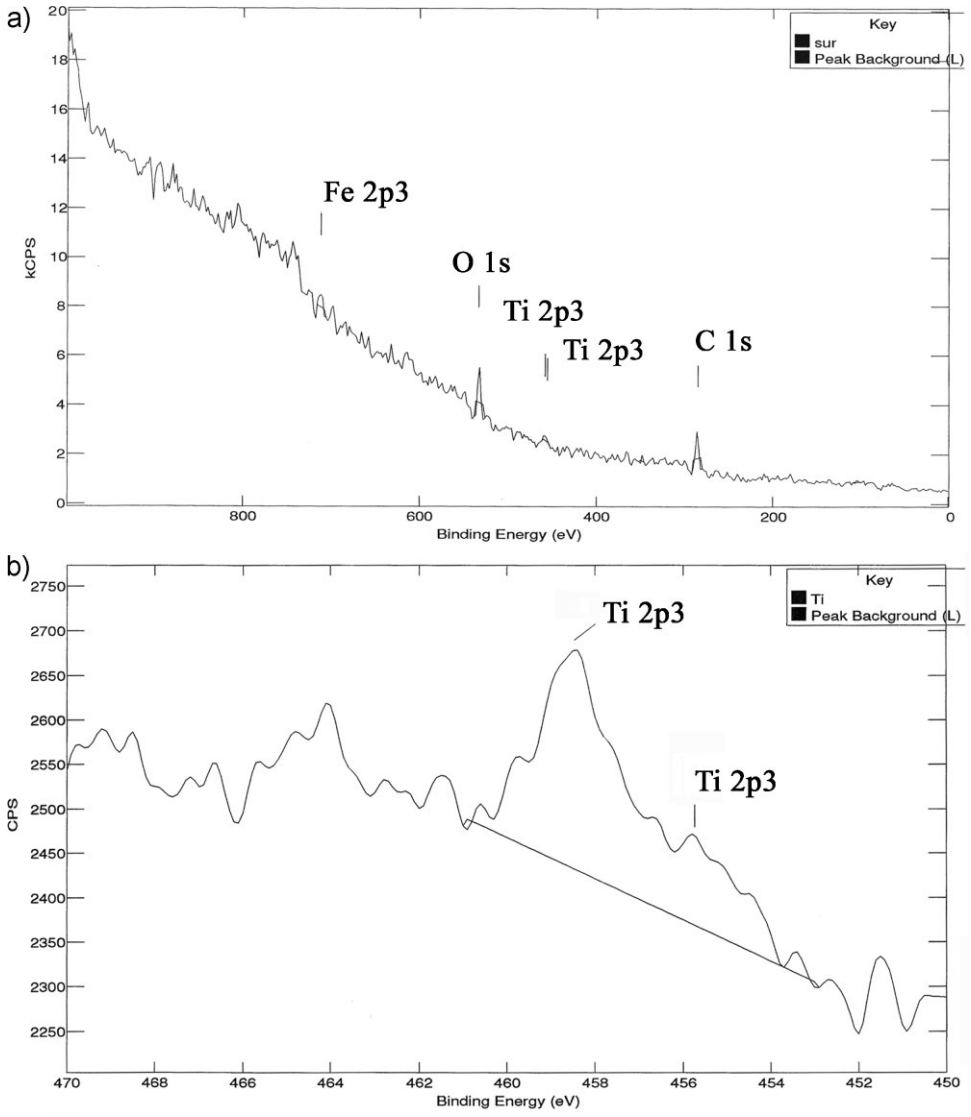

Figure 7. XPS results of the outside wall near the rupture on tube A: (a) all elements, (b) titanium

left less than 0.5 mm gaps in some places of the tubes due to unsymmetrically hydraulically expanding, as seen in Fig. 2. As a result, seawater was provided with access into the shell side from the inlet of the tubes, and simultaneously introducing chloride ions. Then, these chloride ions would particularly accumulate in the gaps between the 78 mm-thick tube sheet and the titanium tubes, and gradually concentrate on the outside wall surfaces of the titanium tubes under the gaps, eventually initiating crevice corrosion [23] as well as galvanic corrosion.

Actually, crevice corrosion is a common degradation on titanium, and has already attracted a wealth of researches to identify its influencing factors [24]. For example, *He* et al. [25] observed that iron content between 0.042 and 0.078% (wt%) would increase the possibility of crevice corrosion on titanium; while *Schutz* [26] designated the threshold temperature for initiation of crevice corrosion on titanium as 70 °C. Come back to our event, in which the content of iron in the titanium tube was about 0.07%, conforming to the opinion of *He* et al. [25]; however, the service temperature was only about 35–40 °C, much lower than the critical temperature. So how could the crevice corrosion occur? This may be ascribed to the complicated environment in the gap of less than 0.5 mm. Let us review the familiar mechanism of crevice corrosion at first. In this electrochemical corrosion, at the beginning, the metal exposed to the air acts as the anode and will be oxidized to cations, while the oxygen within the gap serves as the cathode to be reduced. Once the oxygen is exhausted, this dissolved oxygen reaction ceases. As a result, the potential of the metal under the crevice decreases due to lack of oxygen, and the potential of the metal exposed to the air still remains at a relatively high value. Then, an occluded corrosion cell (OCC) is formed, and will keep attacking the metal under the crevice (i.e., the titanium tube in our event) in an autocatalytic mode with the assistance of the localizedly accumulating hydrochloric acid that is generated by both the hydrolysis of metal cations and the introduction of chloride ions from the environment. All the relevant electrochemical reactions are

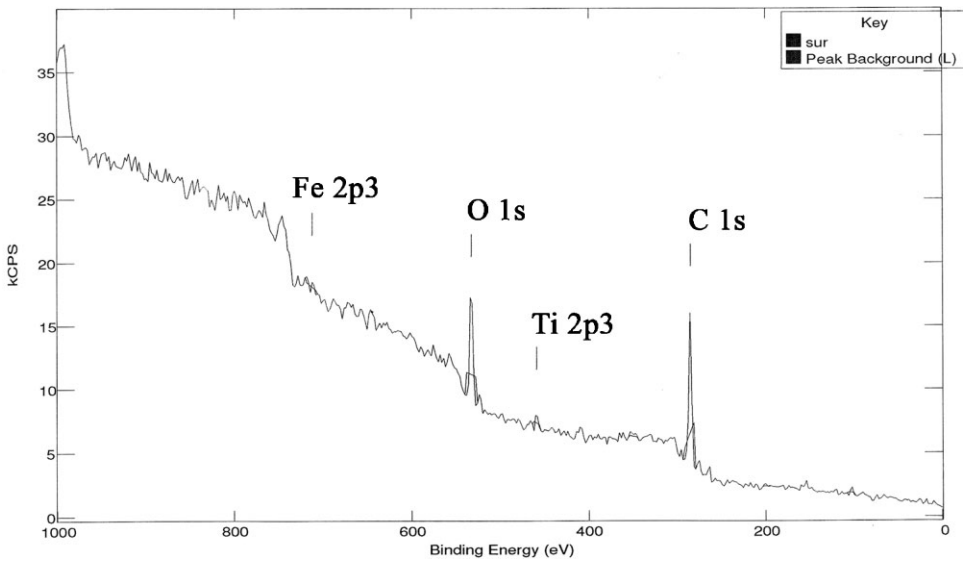

Figure 8. XPS results of the inside wall near the rupture on tube A

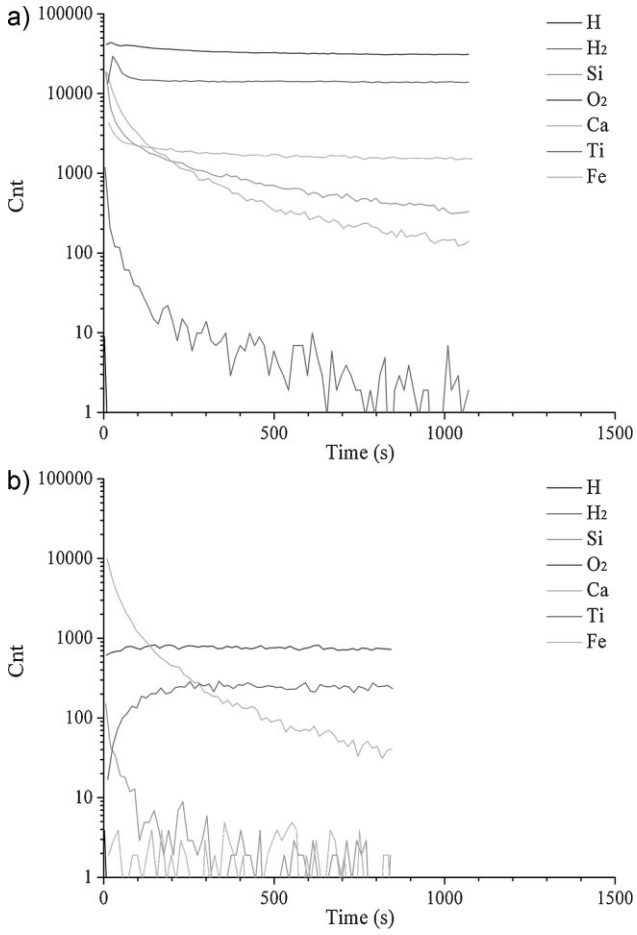

Figure 9. SIMS results of the areas near the rupture on tube A: (a) outside wall, (b) inside wall

demonstrated in Equation (7). As for the initiation temperature, maybe it is true for sole crevice corrosion to take place on titanium at temperatures above 70 °C, however in our event, crevice corrosion was also accompanied by galvanic corrosion, which would probably help to decrease the initial barrier potential for crevice corrosion to occur on titanium. As a result, the threshold temperature is accordingly decreased, at least around 35–40 °C.

$$\begin{aligned} &\text{Anode}: \mathrm{Ti} \rightarrow \mathrm{Ti}^{4+} + 4\mathrm{e} \\ &\text{Cathode}: \mathrm{O_2} + 2\mathrm{H_2O} + 4\mathrm{e} \rightarrow 4\mathrm{OH}^- \\ &\text{Total reaction}: \mathrm{Ti}^{4+}4\mathrm{Cl}^- + 4\mathrm{H_2O} \rightarrow \mathrm{Ti(OH)_4} + 4\mathrm{H}^+\mathrm{Cl}^- \end{aligned} \quad (7)$$

Then, it is easy to infer that, with the progress of both galvanic corrosion and crevice corrosion, metal cations as ferrous ions and titanium ions were continuously produced. Besides forming the corrosion products, these two cations would also hydrolyze in the desalinated water to generate hydrogen ions H^+. When contacting negative electrons, such hydrogen ions will be

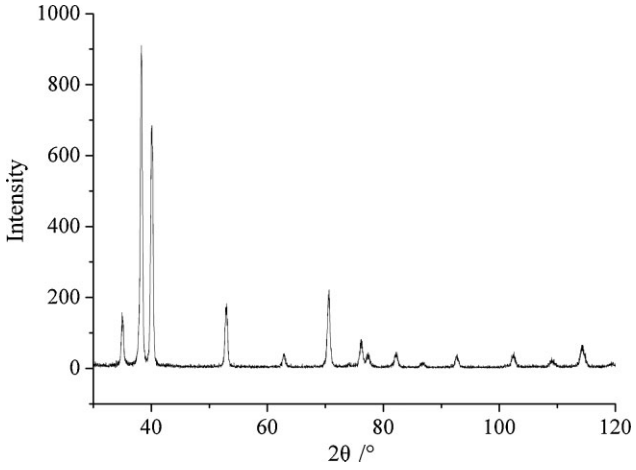

Figure 10. XRD results of the area near the rupture on tube A

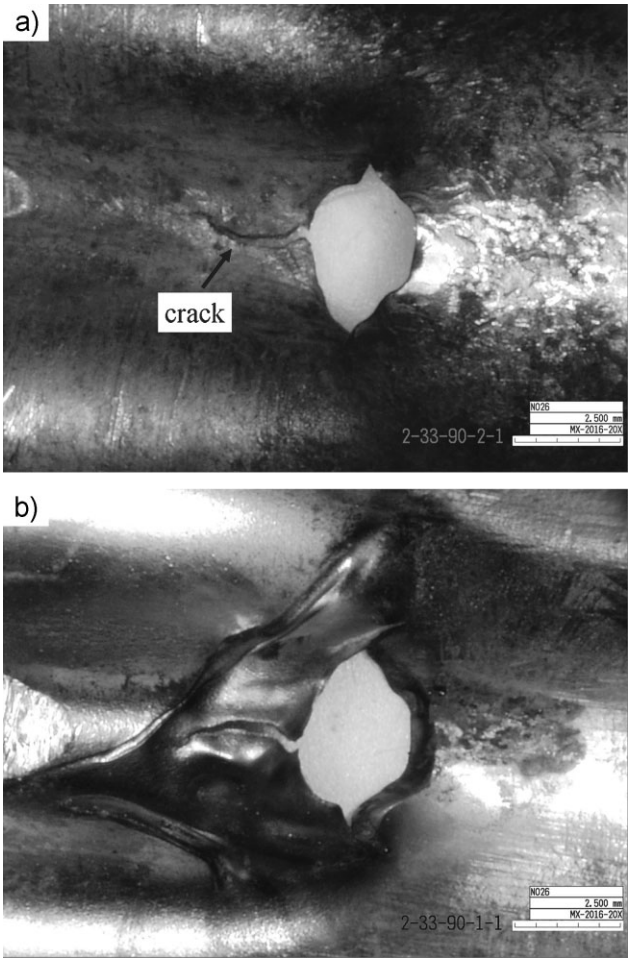

Figure 11. Macroscopic morphologies of the rupture on tube B: (a) outside wall, (b) inside wall

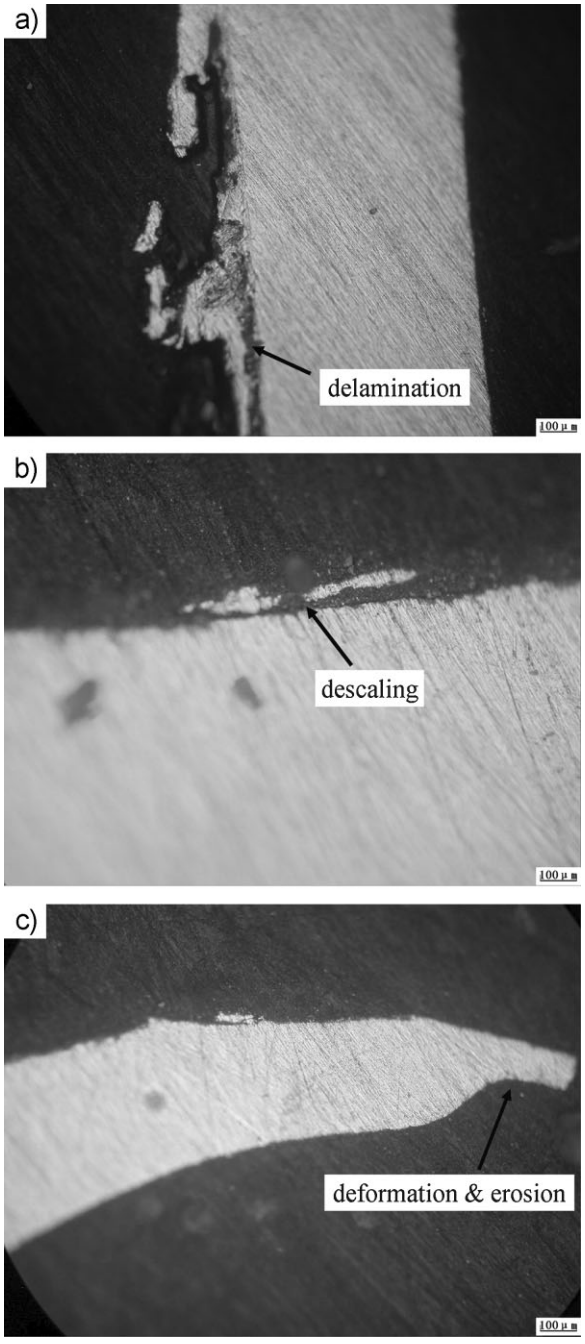

Figure 12. Cross-sections of the rupture on tube B: (a) delamination of matrix material, (b) descaling of matrix material, (c) thinned by erosion

reduced into the hydrogen atoms, seen in Equation (8), and then these hydrogen atoms will be easily absorbed into the titanium matrix material at temperatures above 77 °C [14]. Then, another doubt will be brought about here that the service temperature of the titanium tubes in this event was ranging from 35 to 40 °C, much lower than the threshold value 77 °C, so how could the hydrogen atoms be absorbed? Actually, this critical temperature of 77 °C is only valid in sole Ti–H system. Once alien substances like ferrous ions in this event were introduced, this system would be disturbed, and thus the temperature would be changed. Detailedly speaking, with progress of the galvanic corrosion, the content of ferrous ions kept increasing, hence more and more hydrogen ions would be continuously produced due to hydrolysis, and accordingly the concentration of hydrogen atoms would reach a relatively high value. As a result, the proneness of hydrogen atoms to be absorbed into titanium was facilitated on the basis of Le Chatelier's principle. To sum up, it can be briefly put forward that the threshold temperature for hydrogen atoms to be absorbed into titanium will be decreased with the catalysis effect of ferrous ions, at least around 35–40 °C.

$$H^+ + e \rightarrow H \quad (8)$$

As a matter of fact, this absorption process of hydrogen atoms into titanium is always substantially retarded by the passive film TiO_2 on titanium. Quantificationally, the hydrogen diffusion coefficient in pure titanium is $1.07 \times 10^{-12}\,cm^2/s$, however that value in TiO_2 is only $7.5 \times 10^{-20}\,cm^2/s$ [27]. Consequently, the hydrogen atoms will first be absorbed by the TiO_2, even composing metastable compounds TiO(OH) [Equation (9), [28]] if their contents continuously increase. Then, *Zeng* et al. [28] thought that the hydrogen atoms in TiO(OH) will serve as the

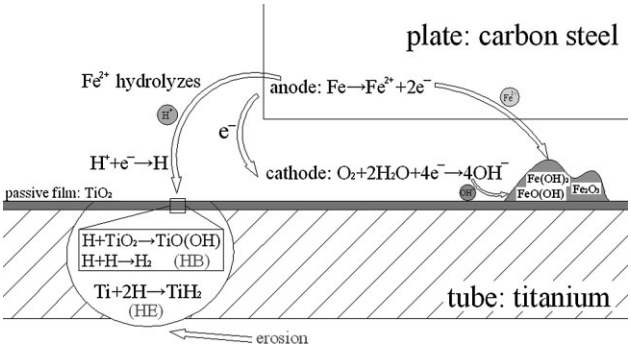

Figure 13. Schematic diagram of the mechanisms of electrochemical corrosions and HAC on titanium tubes

electron donors to produce hydrogen ions, the reverse reaction of Equation (8). However in our opinion, these hydrogen atoms will be mutually coupled and form hydrogen gases H_2, Equation (10). This can be also ascribed to the presence of ferrous ions, which have already yielded relatively high content of hydrogen ions in the system to prohibit the reverse reaction of Equation (8), still the Le Chatelier's principle.

$$H + TiO_2 \rightarrow TiO(OH) \quad (9)$$

$$H + H \rightarrow H_2 \quad (10)$$

What is more, other than mutually coupled to form hydrogen gases within TiO_2, the excessive hydrogen atoms with diameter of 1.06 Å [29] can easily traverse through the TiO_2 crystal structure whose smallest lattice parameter is as ''wide'' as 2.95 Å [30] (even larger than the diameter of hydrogen molecule, 2.72 Å [31]). As a consequence, the hydrogen atoms will quickly diffuse into and within the pure titanium under TiO_2 film until reaching the maximum solubility of 20–100 ppm [28]. This will lead to two results, on one hand, these hydrogen atoms will also be mutually coupled to produce hydrogen gases; on the other hand, the titanium hydride TiH_x will be formed, seen in Equation (11).

$$Ti + xH \rightarrow TiH_x \quad (11)$$

Now we can basically determine the sources of hydrogen that finally resulted in the HAC in this event. With the increasing amount of hydrogen gases within both the TiO_2 and the pure titanium (indeed detected by SIMS), the HB was engendered upon the outside wall of the tubes. As a result, the passive film was destroyed and the tube wall was localizedly bulged inwards the inside wall along the thickness, which was exactly the origin of the 'unknown' force on the outside walls of both tubes A and B. Actually, once the tube wall was bulged, the erosion effect from the seawater containing sediment particles in the tube side would be exerted on this bulge, gradually thinning its wall thickness until perforation. Relevant mechanical mechanisms will be proposed in Part II. Besides the HB induced by hydrogen gases, the other degradation as HE was also aroused by the presence of TiH_x on the titanium tubes in this event. The value of x usually ranges from 1.5 to 2.0 with respect to the thickness of the titanium hydride, and the surface is commonly TiH_2 [32]. TiH_2 is an absolutely brittle compound in fcc (face-centered cubic) structure [33, 34], and its thickness will keep growing with the increase of hydrogen concentration in it. Once the thickness exceeds a critical value, cracks always in brittle mode are brought about [32], i.e. the HE [35], which was distinctly observed in Fig. 11 on the titanium tube with eligible strength and toughness.

Now it can be briefly summarized that since there existed less than 0.5mm gap between the titanium tubes and carbon steel plate due to unsymmetrically hydraulically expanding and unsealed welding on the inlet of tube sheet, galvanic corrosion and crevice corrosion naturally happened in the gap zone under penetration of seawater. Then, the HAC including HB and HE was induced on the outside wall of the tube, leading to a localized bulge inwards to the inside wall of the tube. In the following, the sustaining erosion from seawater containing sediment particles in the tube side was exerted on the bulge. The bulge wall was thus gradually thinned and finally ruptured.

5 Conclusions and recommendations

(i) Matrix materials of the titanium tubes in the RCW heat exchangers were standard Gr.2 pure titanium, qualified in chemical compositions, microstructures, and mechanical properties.

(ii) The unsealed welding to the inlet of the tube sheet naturally left some gaps between the titanium tubes and carbon steel plates because of the unsymmetrically hydraulically expanding. It was such kind of the gaps that resulted in occurrence of galvanic corrosion and crevice corrosion, and then induced the HAC including HB and HE.

(iii) Under such electrochemical corrosions, the titanium tubes were localizedly bulged inwards to the inside wall due to HB and then thinned by erosion from seawater containing sediment particles in the tube side until being ruptured.

(iv) The interaction between galvanic corrosion and crevice corrosion decreased the initiation temperature from 70 °C to 35–40 °C for HAC to occur on titanium, which was a new phenomenon founded in the present study.

Based on cause analysis for this failure, a simple, effective countermeasure was proposed, i.e., special polymer resin sealants must be coated on the inlet surface of the tube sheet to fill possible 0.5 mm gaps between the tubes and the plates. As a result, the galvanic corrosion and crevice corrosion, as well as subsequent HAC were thus eliminated. Afterward, the bulges caused by electrochemical corrosion did not occur any more in the routine inspection of next few years.

Acknowledgements: This work was cooperated with Third Qinshan Nuclear Power Co. Ltd. (TQNPC) and was supported by Shanghai Leading Academic Discipline Project (Project Number: B113).

6 References

[1] Y. Zhou, C. Rengifo, P.-P. Chen, J. Hinze, *Energy Policy* **2011**, *39*, 771.
[2] Q. Wang, *Energy Policy* **2009**, *37*, 2487.
[3] *Qinshan Nuclear Power Plant*, Wikipedia, **2011**, http://en.wikipedia.org/wiki/Qinshan_Nuclear_Power_Plant.
[4] V. G. Snell, *CANDU Nuclear Power Plant Design*, **1999**, http://canteach.candu.org/library/19990101.pdf.
[5] Z.-G. Yang, *Heat Treat. Met.* **2007**, 32(s), 28 (in Chinese with an English abstract).
[6] T. Nguyen, R. Jaitly, K. Dinnie, R. Henry, D. Sinclair, *Nucl. Eng. Des.* **2008**, *238*, 1093.
[7] Y. Gong, Z.-G. Yang, *Mater. Des.* **2011**, *32*, 671.
[8] Y. Gong, C. Yang, C. Yao, Z.-G. Yang, *Mater. Corros.* **2011**, *62*, 967.
[9] Y. Gong, J. Zhong, Z.-G. Yang, *Mater. Des.* **2010**, *31*, 4258.
[10] Y. Gong, Z.-G. Yang, J.-Z. Yuan, *Mater. Corros.* **2012**, *63*, 18.
[11] *Corrosion resistance of titanium*, Titanium metals corporation, http://www.timet.com/pdfs/corrosion.pdf.
[12] *ASME SB-338*-**2007** Specification for seamless and welded titanium and titanium alloy tubes for condensers and heat exchangers.
[13] *ASME SA-515*-**2007** Pressure vessel plates, carbon steel, for intermediate- and higher-temperature service.
[14] *ASME SB-265*-**2004** Specification for titanium and titanium alloy strip, sheet, and plate.
[15] *GB/T 3620 1*-**2007**, Designation and composition of titanium and titanium alloys.
[16] *GB/T 3624*-**1995**, Titanium and titanium alloy tubes.
[17] BE lookup table for signals from elements and common chemical species, Handbook of the Elements and Native Oxides, XPS International Inc., **1999**, http://www.xpsdata.com/XI_BE_Lookup_table.pdf.
[18] Y. Furuya, A. Takasaki, K. Mizuno, T. Yoshiie, *J. Alloy Compd.* **2007**, *446-447*, 447.
[19] H. Züchner, J. Kintrup, R. Dobrileit, I. Untiedt, *J. Alloy Compd.* **1999**, *293-295*, 202.
[20] T. M. Marcelo, V. Livramento, M. V. Oliveira, M. H. Carvalho, *Mat. Res.* **2006**, *9*, 65.
[21] R. W. Revie, H. H. Uhlig, *Corrosion and Corrosion Control: An Introduction to Corrosion Science and Engineering*, 4th Edn. John Wiley & Sons, Inc, Hoboken, NJ, USA **2008**, p. 31.
[22] F. L. LaQue, *Marine Corrosion, Causes and Prevention*, John Wiley & Sons, Inc, Hoboken, NJ, USA **1975**, p. 179.
[23] Y. Gong, J. Cao, X.-H. Meng, Z.-G. Yang, *Mater. Corros.* **2009**, *60*, 899.
[24] L. Yan, J. J. Noël, D. W. Shoesmith, *Electrochim. Acta* **2011**, *56*, 1810.
[25] X. He, J. J. Noël, D. W. Shoesmith, *Corrosion* **2004**, *60*, 378.
[26] R. W. Schutz, *Proc. 6th Int. Conf. on Titanium*, Vol. IV, Cannes, France, **1988**, p. 1917.
[27] B. G. Pound, *Corrosion* **1990**, *47*, 99.
[28] Y. Zeng, J. J. Noël, P. R. Norton, D. W. Shoesmith, *J. Electroanal. Chem.* **2010**, *649*, 277.
[29] R. A. Serway, J. W. Jewett, *Principles of Physics: A Calculus-based text*, Vol. 1, Cengage Learning, Florence, KY **2006**, p. 28.
[30] *Mineral structures and property data of TiO_2 group*, University of Colorado, http://ruby.colorado.edu/~smyth/min/tio2.html.
[31] W. L. Mao, H.-K. Mao, A. F. Goncharov, V. V. Struzhkin, Q. Guo, J. Hu, J. Shu, R. J. Hemley, M. Somayazulu, Y. Zhao, *Science* **2002**, *297*, 2247.
[32] G. Nakayama, Y. Sakakibara, Y. Taniyama, H. Cho, T. Jintoku, S. Kawakami, M. Takemoto, *J. Nucl. Mater.* **2008**, *379*, 174.
[33] V. Bhosle, E. G. Baburaj, M. Miranova, K. Salama, *Mater. Sci. Eng., A* **2003**, *356*, 190.
[34] H. Numakura, M. Koiwa, *Acta Metall.* **1984**, *32*, 1799.
[35] Y.-S. Gu, Y. Gong, Z.-G. Yang, *J. Fail. Anal. Preven.* **2010**, *10*, 399.

(Received: April 20, 2011) W6189
(Accepted: May 17, 2011)